AD-A172 242 CORROSION FATIGUE AND ELECTROCHEMICAL REACTIONS IN MODIFIED HY130 STEEL(U) LEHIGH UNIV BETHLEHEM PA INST OF FRACTURE AND SOLID MECHANICS.. G SHIM ET AL. MAY 86 1/1

UNCLASSIFIED IFSM-86-142 N00014-83-K-0107 F/G 11/6 NL

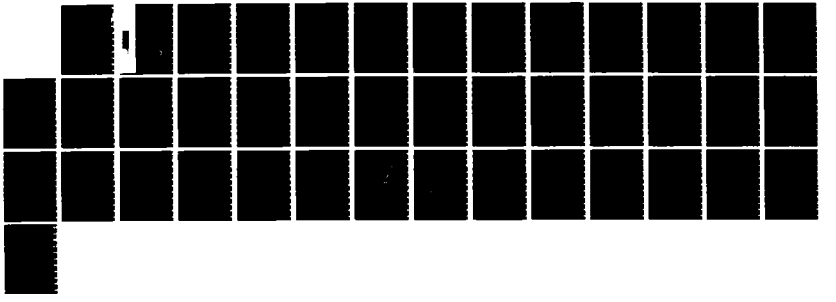

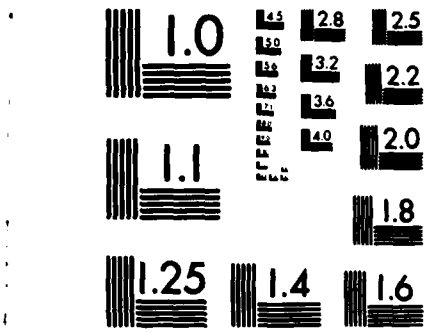
1.0
1.1
1.25
1.4
1.6
1.8
2.0
2.2
2.5
2.8
3.2
3.6
4.0
4.5
5.0

IFSM 86-142

LEHIGH UNIVERSITY

INSTITUTE OF FRACTURE AND SOLID MECHANICS

CORROSION FATIGUE AND ELECTROCHEMICAL REACTIONS IN MODIFIED HY130 STEEL

by

Gunchoo Shim and R. P. Wei

May, 1986

Technical Report No. 18

Office of Naval Research
Contract N00014-83-K-0107, NR 036-097

CORROSION FATIGUE AND ELECTROCHEMICAL REACTIONS IN MODIFIED HY130 STEEL

by

Gunchoo Shim* and R. P. Wei
Lehigh University
Bethlehem, PA 18015

Technical Report No. 18

OFFICE OF NAVAL RESEARCH

*Now with the Korean Institute of Energy and Resources, Energy Laboratory, Chungnam, Korea

UNCLASSIFIED
SECURITY CLASSIFICATION OF THIS PAGE

AD-A172 242

REPORT DOCUMENTATION PAGE

1a. REPORT SECURITY CLASSIFICATION: UNCLASSIFIED	1b. RESTRICTIVE MARKINGS
2a. SECURITY CLASSIFICATION AUTHORITY	3. DISTRIBUTION/AVAILABILITY OF REPORT: This document has been approved for public release and sale; its distribution is unlimited.
2b. DECLASSIFICATION/DOWNGRADING SCHEDULE	
4. PERFORMING ORGANIZATION REPORT NUMBER(S): IFSM 86-142, TR-18	5. MONITORING ORGANIZATION REPORT NUMBER(S)
6a. NAME OF PERFORMING ORGANIZATION: LEHIGH UNIVERSITY; 6b. OFFICE SYMBOL (If applicable)	7a. NAME OF MONITORING ORGANIZATION: OFFICE OF NAVAL RESEARCH
6c. ADDRESS (City, State and ZIP Code): Bethlehem, PA 18015	7b. ADDRESS (City, State and ZIP Code): Department of the Navy, Arlington, VA
8a. NAME OF FUNDING/SPONSORING ORGANIZATION: OFFICE OF NAVAL RESEARCH; 8b. OFFICE SYMBOL (If applicable)	9. PROCUREMENT INSTRUMENT IDENTIFICATION NUMBER: N00014-83-K-0107
8c. ADDRESS (City, State and ZIP Code): Department of the Navy, Arlington, VA	10. SOURCE OF FUNDING NOS. — PROGRAM ELEMENT NO.: ; PROJECT NO.: ; TASK NO.: ; WORK UNIT NO.: NR036-097
11. TITLE (Include Security Classification): CORROSION FATIGUE AND ELECTROCHEMICAL REACTIONS IN MODIFIED HY130 STEEL	
12. PERSONAL AUTHOR(S): Gunchoo Shim and R. P. Wei	
13a. TYPE OF REPORT: Technical; 13b. TIME COVERED: FROM _____ TO _____	14. DATE OF REPORT (Yr., Mo., Day): May, 1986; 15. PAGE COUNT: 39
16. SUPPLEMENTARY NOTATION	
17. COSATI CODES — FIELD: ; GROUP: ; SUB. GR.:	18. SUBJECT TERMS (Continue on reverse if necessary and identify by block number): Corrosion fatigue; Environmental effect; Crack growth; Modeling; Electrochemistry; Fracture mechanics, Steel.

19. ABSTRACT (Continue on reverse if necessary and identify by block number)

Fatigue and electrochemical simulation tests were carried out on a modified HY-130 steel in an acetate buffer solution (pH 4.2) to investigate the relationship between corrosion fatigue crack growth response of high strength steels in aqueous environments and electrochemical reactions at the crack tip. Corrosion fatigue crack growth rates were determined as a function of temperature (276 to 363 K) and frequency (0.03 to 10 Hz) under open circuit conditions. Electrochemical simulation experiments were carried out over the same range of temperatures, and measured the galvanic current transient between a clean and an oxidized surface, and the corresponding mixed potential.

The results strongly suggested electrochemical reaction control of corrosion fatigue crack growth, and showed that hydrogen evolution in this system followed the Volmer-Heyrovsky mechanism. Because of extraneous charges introduced by cathodic cleaning, a definitive correlation and an identification of the rate controlling process could not be made. Methods for alleviating this difficulty are discussed.

20. DISTRIBUTION/AVAILABILITY OF ABSTRACT: UNCLASSIFIED/UNLIMITED ☒ SAME AS RPT. ☐ DTIC USERS ☐	21. ABSTRACT SECURITY CLASSIFICATION: UNCLASSIFIED
22a. NAME OF RESPONSIBLE INDIVIDUAL: Dr. R. P. Wei	22b. TELEPHONE NUMBER (Include Area Code): (215) 861-3587; 22c. OFFICE SYMBOL

DD FORM 1473, 83 APR — EDITION OF 1 JAN 73 IS OBSOLETE.

UNCLASSIFIED
SECURITY CLASSIFICATION OF THIS PAGE

CORROSION FATIGUE AND ELECTROCHEMICAL REACTIONS IN MODIFIED HY130 STEEL

Gunchoo Shim* and R. P. Wei
Department of Mechanical Engineering and Mechanics
and
Center for Surface and Coatings Research
Lehigh University
Bethlehem, PA 18015

ABSTRACT

To investigate the relationship between corrosion fatigue crack growth response of high strength steels in aqueous environments and electrochemical reactions at the crack tip, fatigue and electrochemical simulation tests were carried out on a modified HY-130 steel in acetate buffer solution.

Corrosion fatigue crack growth rates were determined as a function of temperature (276 to 363 K) and frequency (0.03 to 10 Hz) under open circuit conditions. The electrochemical simulation experiments were carried out over the same range of temperatures, and measured the galvanic current transient between a clean and an oxidized surface and the corresponding mixed potential. These experiments were based on the assumption that the newly created surfaces at the crack tip and its neighboring oxidized surfaces formed a localized galvanic cell.

Results from the two sets of experiments strongly suggested electrochemical reaction control of corrosion fatigue crack growth. The electrochemical experiments indicated that hydrogen evolution in this system followed the Volmer-Heyrovsky mechanism. Because of uncertainties associated with extraneous charges introduced by cathodic cleaning of the clean surface, a definitive correlation and an identification of the rate controlling process could not be made. The results and methods for alleviating this difficulty are discussed.

*Now with the Korean Institute of Energy and Resources, Energy Laboratory, Chungnam, Korea

INTRODUCTION

Corrosion fatigue (CF) crack growth of high strength steels in aqueous environments is generally attributed to hydrogen embrittlement in the highly strained region immediately ahead of the crack tip [1,2]. This localized hydrogen embrittlement is considered to be the result of a number of processes operating in sequence, with the rate of crack growth controlled by the slowest process in this sequence. The controlling process in a given system would depend on the material and the environmental conditions.

Recent results on fatigue crack growth in a modified HY130 steel at different frequencies indicated at least two regions of crack growth in the aqueous environments [3]. These results are reproduced in Fig. 1, along with data obtained from separate tests in vacuum ($<10^{-6}$ Pa) and in water vapor (at 40 and 100 Pa). The data in water vapor are shown as a function of equivalent exposure (i.e., pressure divided by twice the frequency, $p_o/2f$) on the left side of Fig. 1, and those in the aqueous environments, on the right, as functions of 1/2f (representing the effective time for reactions during a fatigue cycle). The crack growth rate in water vapor reached a plateau or saturation value which corresponded to the growth rate in the aqueous environments at high frequencies, and to that observed in moist air. This correspondence in fatigue crack growth rates has been observed also by other investigators [4-6]. These observations strongly suggested that corrosion fatigue crack growth in this region is controlled by a common reaction process; namely, the dissociative chemisorption of water on the bare metal surfaces to produce hydrogen [7-9]. With decreases in frequency, further increases in crack growth rates in the aqueous environments towards a second plateau were observed. It is believed that this additional increase (and possible further increases) in growth rate is associated with hydrogen that is produced by the electrochemical reactions at the crack tip, and that the crack growth response is controlled by these reactions.

The objective of this research was therefore to establish a positive correlation between the rates of corrosion fatigue crack growth and the kinetics of electrochemical reactions at the crack tip. Based on the experimental observations, a modified superposition model has been proposed for use in analyzing the corrosion fatigue data, Eqn. (1), for K_{max} below K_{Iscc} [3].

$$(da/dN)_e = (da/dN)_r^* + (da/dN)_{cf} \quad (1)$$

where $(da/dN)_e$ = fatigue crack growth rate in aqueous solution; $(da/dN)_r^*$ = reference crack growth rate in aqueous solution, corresponding to the first plateau; $(da/dN)_{cf}$ = contribution from the second (electrochemical) reaction step; K_{max} = maximum stress intensity factor in a given fatigue loading cycle; and K_{Iscc} = threshold K for stress corrosion cracking. The corrosion fatigue term, $(da/dN)_{cf}$, was assumed by Wei and Shim [3] to be proportional to the amount of hydrogen produced (hence, to the extent of electrochemical reactions each cycle), and is to be directly related to the kinetics of and the time for these reactions. Justification for this assumption is based on previous work on gaseous systems, and is given in [3].

Because it is impossible to make in-situ measurements of electrochemical reaction kinetics at the crack tip during crack growth, simulation techniques must be used. Since the crack-tip potential is not always known and can be quite different from the applied potential, it is difficult to make use of potentiostatic techniques, such as the potential step and the scratching electrode methods. In these techniques the current decay transient is measured under potentiostatic conditions after a clean metal surface is suddenly exposed to an electrolyte. The current transient reflects the rates of the electrochemical reactions, and consequently are to be related to crack growth rates. Clean metal surfaces (i.e., those free of oxide films or corrosion products) are obtained presumably by holding the specimen at a cathodic potential or by mechanically scratching the specimen surface.

These techniques, however, presume that the potential at the crack tip is either the same as that applied at the surface of the fatigue specimen or can be correctly simulated. In practice, however, such is not the case. Even for highly conductive electrolytes, the difference between applied and crack tip potentials may not be negligible. In some cases, solid or gaseous corrosion products may obstruct the ionic path, thereby effectively isolating the crack tip region, and the crack tip potential would be almost independent of the applied potential and be nearly equal to the free corrosion potential [10-14]. The applied potential would then have little or no effect on crack growth rates.

To avoid these difficulties, a new experimental technique is devised to simulate the electrochemical reactions at the crack tip during CF crack growth under open circuit conditions, and is used to examine the relationship between these reactions and crack growth response. This technique is based on the assumption that the clean metal surface at the crack tip and its oxidized surroundings form a localized galvanic cell: the former acting as the anode and the latter as the cathode. The current flow between the two electrodes is expected to reflect the rates of electrochemical reactions during a given fatigue cycle.

The relationship between electrochemical reactions and corrosion fatigue crack growth rates is examined through the temperature and frequency (or time) dependence of these two processes. Temperature affects the kinetics of electrochemical reactions, while frequency determines the time available for these reactions as well as the degree of mechanical pumping of solution into and out of the crack tip region during fatigue. The fatigue crack growth rate in a given aqueous solution is therefore measured as a function of temperature and frequency under a constant-ΔK condition. Electrochemical experiments in the same solution are carried out to determine the kinetics of electrochemical reactions, or more specifically hydrogen evolution reactions, as a function of temperature. The crack growth data are analyzed in terms of a reaction-controlled model [3], and the possibilities of relating these results to the measured

hydrogen evolution kinetics data obtained from the electrochemical experiments are examined.

MATERIAL AND EXPERIMENTAL WORK

Material and Test Environment

A 12.7 mm-thick plate of modified HY130 steel, containing slightly higher amounts of Ni and lower Mn than HY130 steel, was provided by the Research Laboratory of United States Steel Corporation for study. This modified version of HY130 steel is considered to be less susceptible to temper embrittlement, and is termed the "stress-relievable modification" of HY130 steel by the producer. (Unless otherwise specified, the designation of HY130 steel in this paper refers to this modified grade.) The plate was cross-rolled, austenitized at 1090 K, water quenched, and tempered at 880 to 894 K. A 25.4 mm thick plate of regular HY130 steel was also used for some of the preliminary corrosion fatigue tests. The chemical composition and mechanical properties of these steels are given in Tables 1 and 2. The microstructure of the modified HY130 steel was observed to be composed of ferrites and tempered martensites.

An acetate buffer solution (pH = 4.2 at 298 K), consisting of an equivolume mixture of 0.3N glacial acetic acid and 0.137N sodium acetate, was used as the primary electrolyte. This solution was selected because its stable buffering range included values of crack-tip pH reported by Brown et al. [15] and Parrish [16]. For this buffer solution, at pH = 4.2, it was assumed that there would be little difference in pH between the bulk and crack tip electrolytes during fatigue [15,16]. As such, the crack tip conditions can be satisfactorily simulated in a standard electrochemical cell to facilitate the measurement of reaction kinetics. The solution was deaerated with nitrogen before and during the test to remove dissolved oxygen.

Experimental Procedures

Corrosion Fatigue Test

Modified compact tension (CT) specimens, with thickness = 12.6 mm, width = 63.5 mm, and half-height to width ratio (H/W) =

0.6, were used for determining the crack growth kinetics. The orientation of the specimen was LT; that is, with the crack plane normal to the major axis of rolling and the crack growth direction parallel to the long transverse direction of the plate. A 15.9 mm long starter notch was introduced into each specimen by electrospark discharge machining (EDM). All specimens were precracked by fatigue in air. The fatigue precrack was about 9.5 mm from the tip of the starter notch to ensure submergence of the crack tip in the electrolyte during subsequent testing.

Fatigue crack growth tests were conducted under constant ΔK conditions using a computer-controlled closed-loop electrohydraulic testing machine. A compliance method was used to monitor crack growth [17]. The fatigue crack growth rate (da/dN) was obtained by linear regression analysis of the steady-state crack length versus number of elapsed cycle (a vs. N) data for each condition. Uncertainty in the average da/dN value, for a given specimen and ΔK, was within $\pm$ 0.5%. Because of specimen to specimen variations that can be caused by other factors (such as, differences in temperature, specimen alignment, and possible variations in mechanical properties with specimen location), the overall uncertainty was estimated to be $\pm$ 10%.

The crack growth tests were carried out in the acetate buffer solution under open circuit condition. Some of the tests were done under potentiostatic control to examine the effects of applied potential on crack growth rates. To minimize general corrosion and the current needed for maintaining a constant applied potential, the specimens were coated with epoxy, except for narrow surface strips along the anticipated crack path. A Princeton Applied Research (PAR) model 173 potentiostat was used for the potentiostatically controlled tests. For tests under a constant potential, the tip of the Luggin capillary for the Ag/AgCl reference electrode was manually kept close to the advancing crack tip. Two graphite electrodes were used as the counter electrodes. Nylon coated loading pins were used to ensure electrical isolation of the specimen from "ground".

Electrochemical Test

Experimental setup for the electrochemical tests consisted of four major parts: the electrochemical cell containing the electrolyte and electrodes, the zero impedance ammeter which measures the galvanic current [18], the electrometer which measures the mixed potential of the galvanic couple, and the dc power supply for cathodic cleaning of the working electrode (see Fig. 2). The HY130 steel electrode (b), which is maintained clean by cathodic polarization, represents the newly created crack surface at the crack tip, while another HY130 steel electrode (d) with an oxidized surface represents the crack surfaces adjacent to the crack tip. The kinetics of electrochemical reactions in this electrochemical cell, then, would correspond to that of the crack-tip reactions. The experiments essentially involved measuring the current decay when the clean electrode (b) was suddenly coupled with the oxidized electrode (d).

A circular disk of HY130 steel (1 cm^2 in area) was employed as the working electrode (anode), while a cylindrical specimen (1.82 cm^2 in area) of the same steel was used as the counter electrode (cathode) for galvanic coupling. Before each test, the working electrode was polished with 4/0 Emery paper and was cleaned with methanol in an ultrasonic cleaner. After rinsing with distilled water, the specimen was cathodically cleaned in a separate cell, in a borate buffer solution (consisting of an equivolume mixture of 0.15N boric acid and 0.15N sodium borate, at pH = 8.8) to remove air-formed oxides. The specimen was then taken out, rinsed again with distilled water, and was quickly transferred to the main test cell.

Pre-cleaning in the borate buffer solution was necessary because cathodic reduction of air-formed oxides in the acetate buffer solution alone was not effective and failed to give reproducible results. The shape of the specimen holder was such that the specimen surface was covered with water which ensured against exposure to air during transfer from the pre-cleaning cell to the main test cell. After transfer, the specimen was held at -1.7V (Ag/AgCl) to reduce any remaining or new oxides. This double

cleaning procedure provided good reproducibility and was used for all of the electrochemical experiments.

The cylindrical (oxidized) specimen, or the counter electrode, was simply placed in the main cell and allowed to react freely with the solution. With both electrodes in the cell, the working electrode was suddenly switched off from the cleaning circuit and connected to the counter electrode. The resulting current transient between the two electrodes was monitored with the PAR potentiostat (model 173/376) which operated as a zero impedance ammeter [18]. The corresponding transient of the mixed potential of the galvanic couple was also measured with respect to an Ag/AgCl reference electrode (3.0M NaCl filling solution).

EXPERIMENTAL RESULTS

Corrosion Fatigue Test

Reference Crack Growth Rate

Fatigue crack growth rates in vacuum (10^{-6} Pa) at two temperatures, and in 40 Pa water vapor (5Hz) and air (40% Relative Humidity, 10Hz) at room temperature are shown in Fig. 3. The apparent independence of crack growth rates on temperature in vacuum (see Fig. 3), coupled with the experimental evidence [7] showing that the maximum extent of surface reaction between iron and water vapor is also independent of temperature, implied that the saturation crack growth rate in water vapor or in air must be independent of temperature (at least in this temperature range). Although fatigue experiments in water vapor and in air were conducted only at room temperature in this study, the experimental results of Atkinson and Lindley [19], showing no effects of temperature on crack growth rates of A533B-1 steel in air at 293 to 363 K, confirm this implication. These observations support the use of the first plateau crack growth rate (see Eqn. (1)) as the base level, or reference crack growth rate (versus that in vacuum) for assessing the contribution of electrochemical reactions to crack growth.

The asterisk in Fig. 3 denotes the crack growth rate in distilled water at ΔK of 40 MPa-$m^{1/2}$ (10Hz, 296 K). It may be noted that crack growth rates in water vapor and in air at ΔK of 40 MPa-$m^{1/2}$ all fell on the first plateau crack growth rate shown in Fig. 1. The same is true for the crack growth rate in distilled water at 10 Hz. The room temperature crack growth rates in these environments at high frequency, therefore, may be used as the reference rate, $(da/dN)^*_r$, from approximately room temperature up to at least 363 K. In this study, $(da/dN)^*_r$ was found to be 3.18×10^{-7} m/c at ΔK of 40 MPa-$m^{1/2}$ (with R = 0.1).

Effects of Applied Potential on Crack Growth Rates

Constant ΔK tests were also carried out to determine the effects of applied potential on crack growth rates. Tables 3 and 4 show crack growth data at two ΔK levels and two frequencies under various polarization conditions. It may be noted that there was little influence of applied potential; with the crack growth rates under the different applied potentials essentially equal to those at the open circuit potential. These results support the suggestion made by Pickering and coworkers [10-14] that the crack tip remains essentially at the free corrosion potential regardless of applied potential, which probably results from blockage of the electrolytic path by hydrogen bubbles.

Effects of Temperature and Frequency on Crack Growth Rate

The crack growth data obtained in acetate buffer solution as a function of frequency and temperature are shown in Fig. 4. The abscissa is given in 1/2f which is considered to be equivalent to the time available for reactions in a given loading cycle [9]. It may be noted that in this environment increases in temperature caused the crack growth rates to shift to higher frequencies, or to the left. At any given frequency, crack growth rates are faster at higher temperatures indicating at least one of the reaction steps leading to embrittlement of the material is thermally activated.

Galvanic Cell Experiment

Typical galvanic current transients (normalized to peak currents) obtained at several temperatures are shown in Fig. 5. Figure 6 shows several current transients obtained at room temperature in a log-log scale. It may be noted that the reproducibility was very good except near to the end of each test when the surface condition at the anode approached that of the cathode. The initial portion of the current transient, though fairly reproducible, contained information other than that from the anodic reaction process on the clean metal surface. Because the working electrode was cathodically cleaned in-situ before galvanic coupling was made, electrical charge was accumulated in the electrical double layer at the metal-solution interface, as well as in the layer of adsorbed hydrogen, during cleaning. When coupling of the electrodes was made, this accumulated charge was dissipated and contributed to the current transient, along with charge transfer from the anodic reactions that are of interest. The observed current transient, therefore, represented the sum of these currents. This is a key point, and governs the usefulness of the test results. If the accumulated charge during cathodic cleaning is large enough, its discharge can overshadow the current from the anodic reaction process. The galvanic cell experiment then may not properly simulate the electrochemical reactions at the crack tip, and furnish useful information. This point will be discussed later in more detail.

DISCUSSION

Analysis of Electrochemical Data

To facilitate the interpretation of results, the processes that give rise to the observed current and potential transients in the galvanic cell experiment are considered. At any given point during the current transient, the oxidation rate at the anode must equal the reduction rate at the cathode to maintain charge balance. Thus, the current transient may be viewed as a reflection of either the anodic or the cathodic reaction rate, even though the rate would be determined by one or the other

process. Although anodic reactions for iron in acidic solutions have been studied, there is still no consensus on the mechanisms of the oxidation reactions [20-22]. On the other hand, since hydrogen embrittlement is considered to be the mechanism for CF crack growth of HY130 steel in this environment, it is of interest to examine the data in terms of the cathodic partial reaction rate, which is also reflected by the current transient.

The following two mechanisms for hydrogen evolution in acidic solutions are generally accepted [23-25].

I. Volmer-Heyrovsky Mechanism:

$$Fe + H^+ + e^- \rightleftarrows FeH_{ads} \qquad \text{(Volmer Reaction)} \qquad (2)$$

$$FeH_{ads} + H^+ + e^- \rightleftarrows H_2 + Fe \qquad \text{(Heyrovsky Reaction)} \qquad (3)$$

II. Volmer-Tafel Mechanism:

$$Fe + H^+ + e^- \rightleftarrows FeH_{ads} \qquad \text{(Volmer Reaction)} \qquad (4)$$

$$FeH_{ads} + FeH_{ads} \rightleftarrows H_2 + 2Fe \qquad \text{(Tafel Reaction)} \qquad (5)$$

where FeH_{ads} denotes the adsorbed atomic hydrogen. Both mechanisms are examined and are compared with the experimental results.

When the fractional coverage θ by FeH_{ads} is less than 0.2 or greater than 0.8, rate equations can be expressed by Langmuir conditions. However, when the coverage θ is between 0.2 and 0.8, interactions between the adsorbed atoms become appreciable. Temkin [26] proposed that standard free energy of adsorption would decrease linearly with coverage.

$$\Delta G_\theta = \Delta G_o - r\theta \qquad (6)$$

where ΔG_θ and ΔG_o are the standard free energies of adsorption at coverage θ and on the free surface ($\theta = 0$), respectively; and r is a constant. When θ is small, Temkin conditions approach Langmuir conditions.

Volmer-Heyrovsky Mechanism

Assuming that the backward reaction rates are negligible in comparison with the forward reaction rates, the following rate

equations may be written in accordance with Thomas [27].

$$v_1 = k_1(a_H^+)(1 - \theta)\exp\left[-\frac{\alpha F(E - E_r) + \frac{1}{2}\alpha r\theta}{RT}\right] \quad (7)$$

$$v_2 = k_2(a_H^+)\,\theta\,\exp\left[-\frac{\beta F(E - E_r) - \frac{1}{2}\beta r\theta}{RT}\right] \quad (8)$$

where a_H^+ is the activity of hydrogen ions at the electrode surface; E is the potential of the electrode; E_r is the reversible hydrogen potential; F is the Faraday's constant; R is the gas constant, and T is the absolute temperature. The parameters α and β are the symmetry factors of energy barriers ($0 < \alpha < 1$; $0 < \beta < 1$). Since k_1, k_2, a_H^+ and E_r are all constants at a given temperature, they may be grouped into two constants K_1 and K_2.

$$K_1 = k_1(a_H^+)\exp\left[-\frac{\alpha FE_r}{RT}\right] \quad (9)$$

$$K_2 = k_2(a_H^+)\exp\left[-\frac{\beta FE_r}{RT}\right] \quad (10)$$

The mass balance of the adsorbed species can be expressed as follows:

$$\nu(d\theta/dt) = v_1 - v_2 \quad (11)$$

or

$$\nu(d\theta/dt) = K_1(1 - \theta)\exp\left[-\frac{\alpha FE + \frac{1}{2}\alpha r\theta}{RT}\right] - K_2\,\theta\,\exp\left[-\frac{\beta FE - \frac{1}{2}\beta r\theta}{RT}\right] \quad (12)$$

where ν is a constant linking the fractional surface coverage θ to the surface concentration of FeH_{ads} in M/m^2. The quantity ν is considered to be equal to 10^{-4} M/m^2 [28], which corresponds to about one monolayer of surface coverage, or one adsorbed hydrogen (FeH_{ads}) to one surface iron atom.

The total current is given by the following expressions:

$$i = \rho FA(v_1 + v_2) \tag{13a}$$

or

$$i = \rho FA \{K_1(1 - \theta)\exp[-\frac{\alpha FE + \frac{1}{2}\alpha r\theta}{RT}] + K_2\,\theta\,\exp[-\frac{\beta FE - \frac{1}{2}\beta r\theta}{RT}]\} \tag{13b}$$

where A denotes the nominal surface area of the cathode, and ρ is the roughness factor of the cathode.

Volmer-Tafel Mechanism

For this mechanism, the rate equations can be written as follows:

$$v_1 = K_1(1 - \theta)\exp[-\frac{\alpha FE + \frac{1}{2}\alpha r\theta}{RT}] \tag{14}$$

$$v_2 = K_2\,\theta^2 exp[-\frac{\beta r\theta}{RT}] \tag{15}$$

The equation for mass balance is given by Eqn. (16).

$$\nu(d\theta/dt) = 2v_1 - v_2 \tag{16}$$

The factor "2" comes in because the partial step in Eqn. (4) must occur twice to satisfy the requirements of Eqn. (5). Since the reaction step given by Eqn. (5) is purely chemical in nature, the current comes only from the first step given by Eqn. (4).

$$i = \rho FAv_1 \tag{17}$$

Comparison with Experimental Data

If hydrogen evolution occurs by the Volmer-Heyrovsky mechanism, Eqn. (13b) should adequately describe the experimentally observed current and potential transients. To obtain the current i in Eqn. (13b), it is necessary to first solve for θ from Eqn. (12). This was done numerically for all possible combinations of the Volmer-Heyrovsky and Volmer-Tafel mechanisms. The results showed that only the coupled (equally rate limiting)

Volmer-Heyrovsky mechanism was consistent with the experimental data. By incorporating this finding from the numerical analysis as simplifying assumptions, an approximate analytical solution can be obtained (see Appendix), and used to facilitate comparison. The approximate analytical results are shown by following equations:

$$\theta = \frac{1}{2}\{1 - \exp[-\frac{K_1}{\nu}\int_0^t \exp(-\alpha FE/RT)dt]\} \quad (18)$$

$$i = \rho FAK_1 \exp(-\alpha FE/RT) \quad (19)$$

or

$$E = \frac{RT}{\alpha F}(\ell n\ \rho FAK_1 - \ell n\ i) \quad (20)$$

Equation (20) shows that the potential (E) and the logarithm of the current (ℓn i) have a linear relation with a slope of $RT/\alpha F$, which is the steady state cathodic Tafel slope for the Volmer-Heyrovsky mechanism [27,29].

Following Flitt and Bockris [30], a value of 1/3 was assumed for α and β. The slope $RT/\alpha F$ was then calculated for several temperatures and is shown with the experimental data (Fig. 7). Although α and β are usually assumed to be 1/2, Thomas [27] pointed out that there is no reason why they should not have values other than 1/2, and Flitt and Bockris [30] showed a value of 1/3 provided better agreement with experimental data on hydrogen evolution from 0.2C steel in 0.4M H_2SO_4 solution. Figure 7 shows good agreement between these theoretical slopes and the actual experimental data at four different temperatures. The value of K_1 at each temperature determines the vertical position of each straight line. Conversely, K_1 can be determined from experimental data by a linear regression analysis using Eqn. (20) as the fitting function. This is justified by the match between the slopes predicted by Eqn. (20) and the data. It was found that K_1 followed an Arrhenius relationship (Fig. 8), with an estimated activation energy for the Volmer reaction (formation of FeH_{ads} by hydrogen ion discharge) of about 43.7 ± 1.2 kJ/M. Since K_2 was assumed to be equal to K_1 (see Appendix), it fol-

lowed that the activation energy for the Heyrovsky reaction (i.e., the electrochemical desorption of hydrogen) was also equal to about 43.7 ± 1.2 kJ/M.

Figure 7 shows that the linear relation breaks down at the less negative (or less cathodic) potentials, especially at higher temperatures. One possible reason for this breakdown is that the backward reaction rates in both the Volmer and the Heyrovsky reactions were ignored in deriving Eqn. (20). As the surface conditions of the anode and the cathode approached each other, the potential difference between them became small, and the backward reactions became significant and could not be ignored. Because of higher reaction rates, the deviation occurred sooner at the higher temperatures. A second possibility is the breakdown of the simpler Langmuir relationship (versus Temkin's relation) at the higher coverages. The deviation from linearity, observed at the more negative potentials at 273 K, however, is not understood.

As a further comparison, current as a function of time can be computed by Eqn. (20) from the observed potential E versus time data. In Figure 9 these computed results are shown as open symbols superimposed on the observed current transients which are shown as solid curves. Again, the agreement is excellent until deviation from the assumptions for Eqn. (20) became significant.

The agreement between the observed $\ell n\ i$ vs. E slope and the steady state Tafel slope may be explained by the concept proposed originally by Eyring and coworkers [31-33] in their study of the potential transients that resulted from sudden straining of metals in aqueous solutions, and may be best described in terms of the conventional polarization curves (Fig. 10). Prior to coupling, the counter electrode is at the corrosion potential of the system, with the rate of oxidation equal to that of reduction, and the steady state anodic and cathodic polarization curves of the system are shown in Fig. 10 as curves a_4 and c, respectively. When coupling is made, however, the anodic reaction rate increases enormously because of the large fresh anodic

area provided by the clean working electrode. This increase in area is akin to the production of new surfaces by sudden straining. On the other hand, the cathodic area and so also the cathodic reaction rate remain essentially unchanged. As a result, the anodic polarization curve moves far to the right (curve a_1), while the cathodic curve remains at the same position. As the surface condition of the clean electrode approaches steady state, the anodic curve shifts back to the original position. The shift of the mixed potential is, in this sense, the shift of corrosion potential towards a steady state corrosion potential. Since the intersection point is considered to move along the cathodic polarization curve, the slope of the observed ℓn i vs. E curve should match the Tafel slope.

Two possible reasons may be offered to account for the observed deviation of the experimental data from the linear relation given by Eqn. (20)) at long times. The first reason, given earlier, is that the backward reaction rates in the Volmer and the Heyrovsky reactions became significant as the mixed potential approached the corrosion potential of the system. The second reason is that the measured current did not represent the total current available from the anodic process. As the anode became oxidized, a portion of the current would flow to the oxidized region which acted as another cathode, and would not have been measured. The measured potential, being the mixed potential, was not subjected to this difficulty and the predicted current tended to be higher than the measured current, particularly at long times when the cathodic area on the specimen surface became large (Fig. 9). This effect, however, is not expected to be significant when the anodic area is small in relation to the cathodic area; which would be the case at the crack tip.

In summary, it was found that the observed currents and potential transients could be adequately described by the Volmer-Heyrovsky mechanism. A similar analysis has been made for the Volmer-Tafel mechanism. The results suggested, however, that

the Volmer-Tafel mechanism was not applicable to the system used in this study.

Electrochemical Reaction Kinetics and $(da/dN)_{cf}$ Correlation

The corrosion fatigue experiments showed that the growth rates exhibited two regimes of response with changing frequency. The first regime is purely chemical in nature, and is attributed to the reaction of water molecules with (or initial adsorption on) the clean metal surface at the crack tip. The second regime is electrochemical in nature, and is strongly dependent on frequency and temperature. The crack growth rate increased with decreasing frequency, reaching an apparent plateau (or saturation) at low frequencies. With increasing temperature, the overall response shifted to higher frequencies, although the plateau rate remained essentially unchanged. These results are consistent with a model for electrochemical reaction controlled fatigue crack growth [3], with an apparent activation energy of 35.5 ± 7.2 kJ/M. This apparent activation energy for crack growth compared well with 43.7 ± 1.2 kJ/M for the Volmer reaction (formation of FeH_{ads} by hydrogen ion discharge) of the Volmer-Heyrovsky hydrogen evolution mechanism (see Fig. 9). Since $(da/dN)_{cf}$ was assumed to be proportional to the amount of hydrogen entering the steel [1-3], which is in turn proportional to the surface coverage by atomic hydrogen, this match in activation energies appears to indicate a direct correlation between $(da/dN)_{cf}$ and the hydrogen ion reduction reaction.

This apparent correlation, however, fails to identify unambiguously which reaction (cathodic or anodic) is actually in control. If the cathodic reaction rate is slower than the anodic reaction rate, crack growth rate will be controlled by the former. On the other hand, if the anodic reaction is slower, it will control the overall reaction, and the observed activation energy for the formation of FeH_{ads} would not be representative of the process, but would reflect the temperature dependence of the anodic process. Because these reactions are coupled, even if the cathodic reaction were rate controlling, the extent of cathodic

reaction will still be limited by the anodic reactions at the fresh metal surface.

If the galvanic cell experiment truly simulated the reactions at the crack tip, then the kinetic data thus obtained may be used to predict the corrosion fatigue crack growth response. In the galvanic cell experiment the clean metal surface was obtained by cathodic cleaning, which caused an accumulation of extraneous charges on the working electrode. These extra charges, on the other hand, would not be present on the crack tip surfaces under open circuit condition. In the galvanic cell experiment, these extra charges would be transferred and would contribute to the total current. Depending on the relative contributions of charges from cathodic cleaning and from the whole reaction process, the galvanic cell experiment may or may not properly simulate the electrochemical reaction at the crack tip.

Four possible situations may be envisioned and are illustrated in Fig. 11, where $E.e^-$ represents the extra charges; A, charges available from the anodic process; and C, charges consumed by the cathodic process. The width of the connecting passages depicts schematically how fast electrons from each reservoir are supplied or consumed; that is, the reaction rate of each process. The rate of supply of electrons must be equal to the rate of consumption in the overall process.

In Cases 1 and 2, the total reaction rate is assumed to be controlled by the cathodic reaction rate, which is the slowest. For these cases, the kinetics of the hydrogen evolution reaction would be measured correctly by the galvanic cell experiment, irrespective of the presence of the extraneous charges, and can be directly related to the crack growth kinetics. The extent of reaction (which would have been limited by the anodic reaction), however, would be affected. In Case 3, the amount of extraneous charges is assumed to be small, and would be exhausted in a very short time. The remaining current would then reflect the coupling between the anodic and the cathodic reactions, and is

assumed to be controlled by the anodic reaction rate. In this case, the galvanic cell experiment would still adequately represent the crack tip reactions, except at the very beginning when the extra charges are being dissipated. In Case 4, the extraneous charges are assumed to be more than that available from the anodic reaction process, and represent the primary source of electrons. The anodic reaction process (even if it would be rate-controlling) would be overshadowed by the initial transfer of these extra charges. In essence, the cathodic process would appear to be in control. The galvanic cell experiment then would not properly simulate the reactions at the crack tip, and the resulting correlation with crack growth would be fortuitous.

The experimental results now suggest that the extraneous charges due to cathodic cleaning may have been excessive, and the results could not be used to make a positive correlation between the electrochemical kinetics and crack growth response, particularly with respect to the rate controlling process. Resolution of this uncertainty must be made to arrive at a more complete understanding of the role of electrochemical reactions in corrosion fatigue. Nevertheless, it should not be overlooked that the galvanic cell experiment was shown to be adequate for obtaining information on hydrogen evolution kinetics, and provided identification of the Volmer-Heyrovsky reactions as the mechanism for hydrogen evolution in this acidic electrolyte.

Since the extraneous charges were introduced by cathodic cleaning, an obvious way of alleviating the problem is to produce the clean metal surface by mechanical means. A modified scratching electrode method may be used, whereby a masked working electrode is coupled to the freely corroding cathode and then scratched to expose fresh metal surfaces. Alternatively, a specimen may be fractured inside the electrochemical cell to generate the requisite clean surfaces. These possibilities are being explored.

SUMMARY

Corrosion fatigue behavior of a modified HY130 steel in aqueous environments was studied as a function of frequency and temperature at ΔK of 40 MPa-$m^{1/2}$. Two regimes of reaction-controlled corrosion fatigue crack growth were found; one, purely chemical and the other, electrochemical in nature. Major enhancement in crack growth rates was associated with the latter regime. This second regime was shown to depend strongly on temperature and frequency. These results are consistent with a model for surface/electrochemical reaction controlled fatigue crack growth.

A new electrochemical measurement technique was devised to investigate the correlation between crack growth response and electrochemical reaction kinetics. The technique was intended for simulating the electrochemical reactions at the crack tip during corrosion fatigue under open circuit conditions. Analysis of the experimental results obtained by this technique showed that hydrogen evolution in modified HY130 steel in acetate buffer solution (pH = 4.2) proceeded by the Volmer-Heyrovsky mechanism (rather than by the Volmer-Tafel mechanism). The apparent activation energies for the Volmer reaction (formation of FeH_{ads} by hydrogen ion discharge) and the subsequent Heyrovsky reaction (electrochemical desorption of adsorbed hydrogen) were found to be 43.7 ± 1.2 kJ/M.

The match between the activation energy for the Volmer-Heyrovsky reactions and that for corrosion fatigue crack growth of 35.5 ± 7.2 kJ/M [3], suggested a correlation between these two processes. However, because of uncertainties introduced by the accumulated charges during cathodic cleaning in the simulation experiment, no definitive correlation or identification of the rate controlling process (anodic or cathodic) could be made. In-situ breaking of a specimen inside the electrochemical cell and the use of a modified scratching electrode method are being considered to alleviate this difficulty. The evidence for electrochemical reaction control of corrosion fatigue crack growth, though must be viewed as being circumstantial, is compelling.

APPENDIX

The rate equations for the electrochemical desorption mechanism given (Eqns. (7) and (8)) are written for Temkin conditions. To facilitate comparison with experimental data, however, the simpler Langmuir conditions were assumed in place of Temkin conditions at low coverages (less than about 0.4) [27,30]]. Then the term $1/2(\alpha r\theta)$ may be neglected. Following the literature, further simplification can be made by assuming $\alpha = \beta$. Equations (7) and (8) then may be rewritten as follows:

$$v_1 = K_1(1 - \theta)\exp(-\alpha FE/RT) \tag{A1}$$

$$v_2 = K_2\,\theta\,\exp(-\alpha FE/RT) \tag{A2}$$

If the first and the second reaction steps are coupled and are equally rate limiting at steady state, i.e., if v_1 equals v_2, then the following equation may be written:

$$K_1(1 - \theta_s) = K_2\theta_s$$

or

$$K_2/K_1 = (1 - \theta_s)/\theta_s = c \tag{A3}$$

The quantity θ_s is the hydrogen coverage at the steady state, and c is a constant. The mass balance and the current equations are given as follows:

$$\nu(d\theta/dt) = v_1 - v_2 \tag{A4}$$

$$i = \rho FA(v_1 + v_2) \tag{A5}$$

Substituting Eqn. (A3) into Eqns. (A4) and (A5), the following expressions for i and $\nu(d\theta/dt)$ are obtained:

$$\nu(d\theta/dt) = K_1\exp(-\alpha FE/RT)\,[1 - (c + 1)\theta] \tag{A6}$$

$$i = \rho FAK_1\exp(-\alpha FE/RT)\,[1 + (c - 1)\theta] \tag{A7}$$

Solving Eqn. (A6) for θ and substituting into Eqn. (A7) yields:

$$\theta = \frac{1}{c + 1}\left\{1 - \exp\left[-\frac{K_1}{\nu}\int_0^t \exp(-\alpha FE/RT)dt\right]\right\} \tag{A8}$$

$$i = \rho F A K_1 \exp\left(-\frac{\alpha F E}{RT}\right)\{1 + (c - 1)[1 - \exp(-\frac{K_1}{\nu}\int_0^t \exp(-\alpha F E/RT)dt)]\} \quad .....(A9)$$

For the simplest case, i.e., $K_1 = K_2$ or $c = 1$, Eqns. (A8) and (A9) reduce to the following forms:

$$\theta = \frac{1}{2}\{1 - \exp[-\frac{K_1}{\nu}\int_0^t \exp(-\alpha F E/RT)dt]\} \quad (A10)$$

$$i = \rho F A K_1 \exp(-\alpha F E/RT)$$

or

$$E = \frac{RT}{\alpha F}(\ell n\ \rho F A K_1 - \ell n\ i) \quad (A11)$$

ACKNOWLEDGEMENT

Support of this research by the Office of Naval Research under Contract N00014-83-K-0107, NR 036-097 is gratefully acknowledged. The authors also wish to express their appreciation to Drs. A. Alavi, R. D. Granata and G. W. Simmons for their assistance and valuable discussions in connection with the electrochemical experiments, and to the United States Steel Corporation for providing the modified HY-130 steel used in this study.

REFERENCES

1. A. R. Troiano, Trans. ASM 52, 54, 1960.
2. B. E. Wilde, Corrosion 27,(8), 326, 1971.
3. R. P. Wei and G. Shim, ASTM STP 801, ASTM, 5, 1983.
4. J. M. Barsom, Investigation of Subcritical Crack Propagation, Ph.D. Thesis, College of Engineering, University of Pittsburgh, June 1969.
5. E. J. Imhof and J. M. Barsom, ASTM STP 536, ASTM, 182, 1973.
6. R. P. Wei, P. S. Pao, R. G. Hart, and T. W. Weir, J. Engineering Materials and Technology, Trans. ASME, 101, (3), 199, July 1979.
7. D. J. Dwyer and G. W. Simmons, Surface Science, 69, 617, 1977.

8. T. W. Weir, G. W. Simmons, R. G. Hart, and R. P. Wei, Scripta Metallurgica, 14, (3), 357, March 1980.

9. R. P. Wei and G. W. Simmons, in FATIGUE: Environment and Temperature Effects, John J. Burke and Volker Weiss, eds., Sagamore Army Materials Research Conference Proceedings, 27, 59, 1983.

10. B. G. Ateya and H. W. Pickering, in Hydrogen in Metals, ASM, 207, 1974.

11. H. W. Pickering and P. J. Byrne, J. Electrochem. Soc., 120, 607, 1973.

12. B. G. Ateya and H. W. Pickering, J. Electrochem. Soc., 122, 1018, 1975.

13. D. Harris and H. W. Pickering, in Hydrogen Effects on Behavior of Materials, A. W. Thompson and I. M. Bernstein, eds., AIME, NY, 229, 1976.

14. P. Doig and P. E. J. Flewitt, Met. Trans. A, 9A, 357, March 1978.

15. B. F. Brown, C. T. Fujii, and E. P. Dahlberg, J. Electrochem. Soc., 116, (2), 218, February 1969.

16. P. A. Parrish, C. T. Lynch, H. B. Kirkpatrick, and A. Pigeaud, Proc. 1972 Tri-Service Conference on Corrosion, Houston, TX, December 1973.

17. A. Saxena and S. J. Hudak, Jr., Int. J. Fract. Mech., 14, 453, October 1978.

18. G. Lauer and F. Mansfeld, Corrosion, 26, 504, 1970.

19. J. D. Atkinson and T. C. Lindley, in Influence of Environment on Fatigue, IMechE/SEE Joint Conference, London, 65, 1977.

20. J. O'M. Bockris, D. Drazic, and A. R. Despic, Electrochimica Acta, 4, 325, 1961.

21. G. Bech-Nielsen, Electrochimica Acta, 23, 425, 1978.

22. H. Schweickert and W. J. Lorenz, J. Electrochem. Soc., 127, (8), 1693, 1980.

23. T. Erdey-Gruz and M. Volmer, Z. Physik Chem., A150, 203, 1930.

24. J. Heyrovsky, Rec. Tran. Chim. Pays-Bas, 46, 582, 1929.

25. J. Tafel, Z. Physik. Chem. 50, 641, 1905.

26. M. Temkin, Zh. Fiz. Khim., 15, 296, 1941; cf. M. Temkin and V. Pyzhev, ibid., 13, 851, 1939.; Acta Phys.-Chim., URSS, 12, 327, 1940.

27. J. G. N. Thomas, Trans. Farad. Soc., 57, (9), 1603, September 1961.

28. M. Keddam, O. R. Mattos and H. Takenouti, J. Electrochem. Soc., 128 (2), 257, 1981.

29. J. McBreen and M. A. Genshaw, in Fundamental Aspects of Stress Corrosion Cracking, NACE, 51, 1967.

30. H. J. Flitt and J. O'M. Bockris, in Environmental Degradation of Engineering Materials in Hydrogen, Conf. Proc., M. R. Louthan, Jr., R. P. McNitt and R. D. Sisson, Jr., eds., Virginia Polytechnic Institute, 13, 1981.

31. A. G. Funk, J. C. Giddings, C. J. Christensen and H. Eyring, Proc. Natl. Acad. Sci., 43, 421, 1957.

32. A. G. Funk, J. C. Giddings, C. J. Christensen, and H. Eyring, J. Phy. Chem., 61, 1179, 1957.

33. J. C. Giddings, A. G. Funk, C. J. Christensen, and H. Eyring, J. Electrochem. Soc., 106, 91, 1959.

Table 1 : Chemical composition of HY130 and modified HY130 steel.

	C	Mn	P	S	Si	Ni	Cr	Mo	V	Al	N	O
HY130	0.11	0.85	0.004	0.004	0.33	5.00	0.54	0.55	0.060	0.018		
Mod. HY130	0.10	0.35	0.007	0.004	0.23	5.33	0.49	0.57	0.064	0.020	0.012	48ppm

Table 2 : Mechanical properties of HY130 and modified HY130 steel

		Y.S.(0.2 Offset) MPa	T.S. MPa	Elongation %	R.A. %	Charpy V 255K, J
HY130		947	974	21.8		
Mod. HY130	Long.	979	1014	22	68.4	117
	Trans.	986	1027	21	65.7	94.9

Table 3 : Crack growth rates in acetate buffer solution under potentiostatic conditions at ΔK of 40 MPa-$m^{1/2}$. 10^{-7}m/c

E (mV)	0.1 Hz	1 Hz
open	9.14	4.12
-2000		4.04
-1100		4.06
-1000	8.71	
- 800		4.24
- 600		4.17
- 500	9.19	
- 300	8.81	
- 200		4.29
+ 250	8.48	
+ 450		4.14

Table 4 : Crack growth rates in acetate buffer solution under potentiostatic conditions at ΔK of 22 MPa-$m^{1/2}$. 10^{-7}m/c

E (mV)	0.1 Hz	0.5 Hz
open	3.20	1.80
-1000	3.12	1.80
- 300	3.00	

FIGURE CAPTIONS

Figure 1: Comparison of crack growth data obtained in distilled water and in acetate buffer solution as a function of frequency (right side of figure) with those obtained in vacuum and in water vapor (left side) at room temperature (ΔK = 40 MPa-$m^{1/2}$), which shows the continuous nature of cracking response.

Figure 2: Instrument for monitoring galvanic current and potential.

Figure 3: Crack growth data for modified HY130 steel in 40 Pa water vapor, in air, and in vacuum at 293 and 373 K. (R = 0.1 and f = 5 Hz).

Figure 4: Correlation between crack growth rates and the fractional surface coverage by atomic hydrogen.

Figure 5: Semi-logarithmic representation of galvanic current transients at several temperatures.

Figure 6: Galvanic current transients at 297 K.

Figure 7: Current-potential relation during the transient.

Figure 8: Temperature dependence for corrosion fatigue crack growth and for the Volmer reaction in buffered acetate solution.

Figure 9: Comparison between measured current transients (solid curves) and the computed values from the measured potentials (open symbols).

Figure 10: Schematic diagram illustrating the current-potential relation during a transient.

Figure 11: Four possible cases of the galvanic cell experiment with cathodic cleaning to obtain a clean surface.

$E.e^-$: extraneous electrons accumulated by the cleaning process.
A : anodic reaction process.
C : cathodic reaction process.

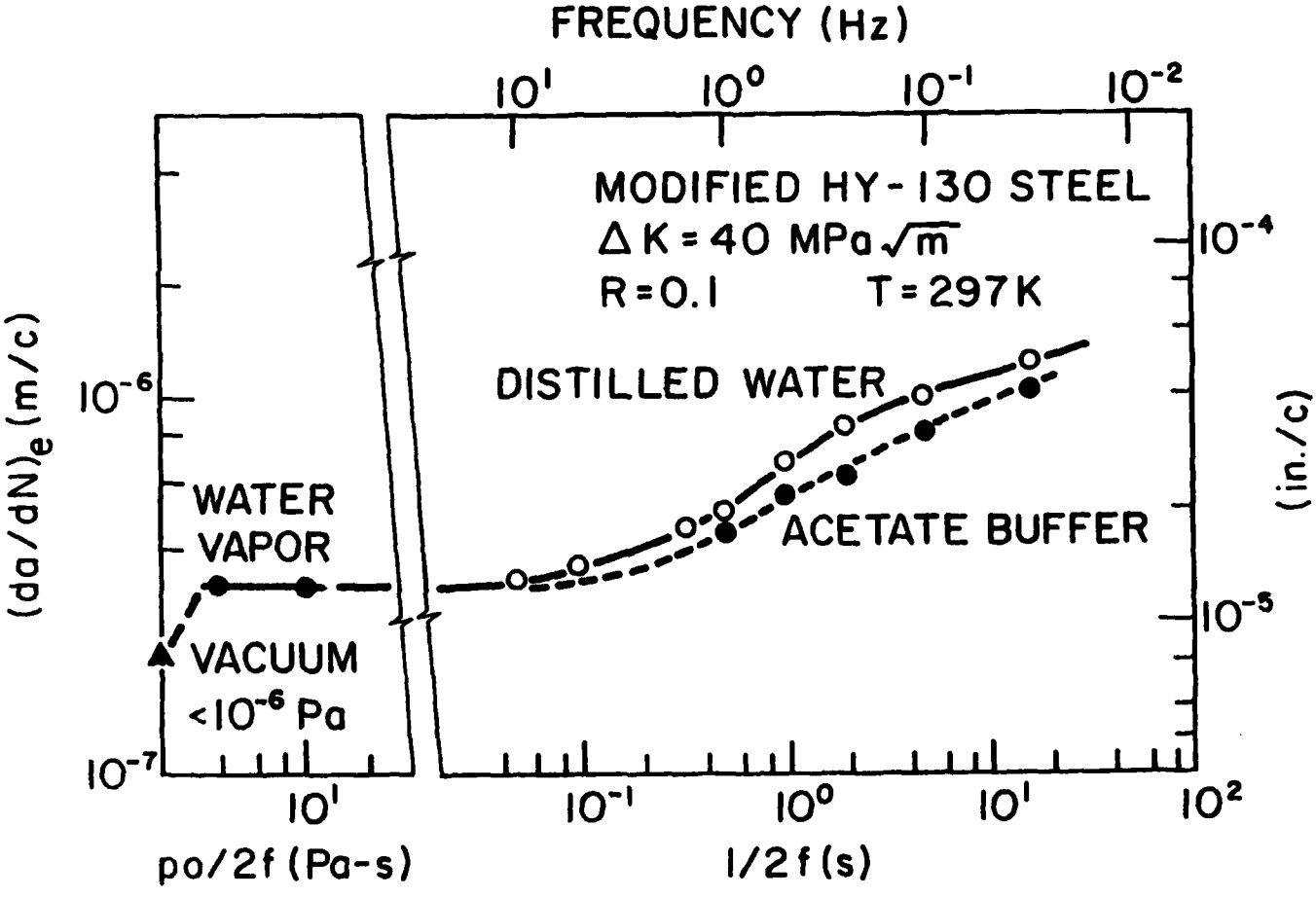

Figure 1: Comparison of crack growth data obtained in distilled water and in acetate buffer solution as a function of frequency (right side of figure) with those obtained in vacuum and in water vapor (left side) at room temperature (ΔK = 40 MPa-$m^{1/2}$), which shows the continuous nature of cracking response.

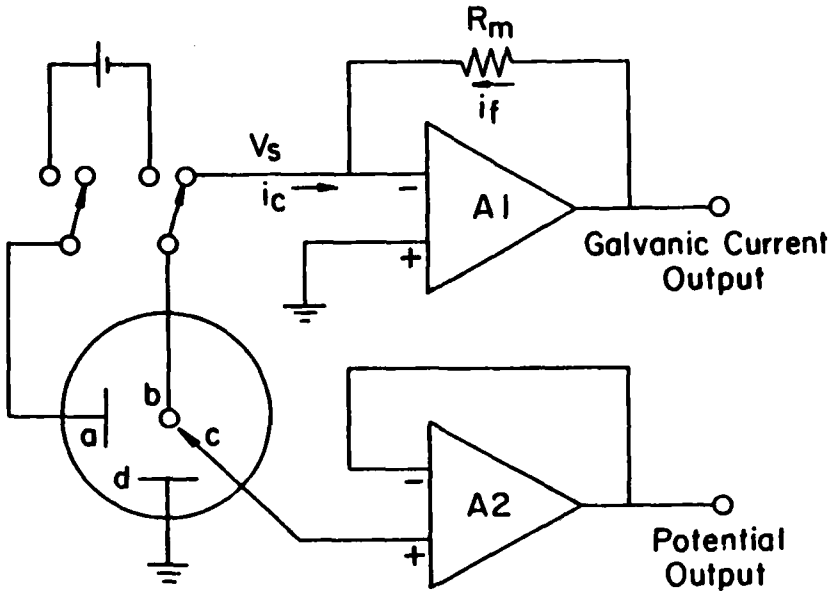

a - counter electrode for cleaning (graphite)

b - working electrode (clean HY130)

c - reference electrode (Ag/AgCl)

d - counter electrode for galvanic coupling (freely corroding HY130)

v_s - voltage, referred to ground

i_c - cell current

i_f - feedback current

R_m - feedback resistance

Figure 2: Instrument for monitoring galvanic current and potential.

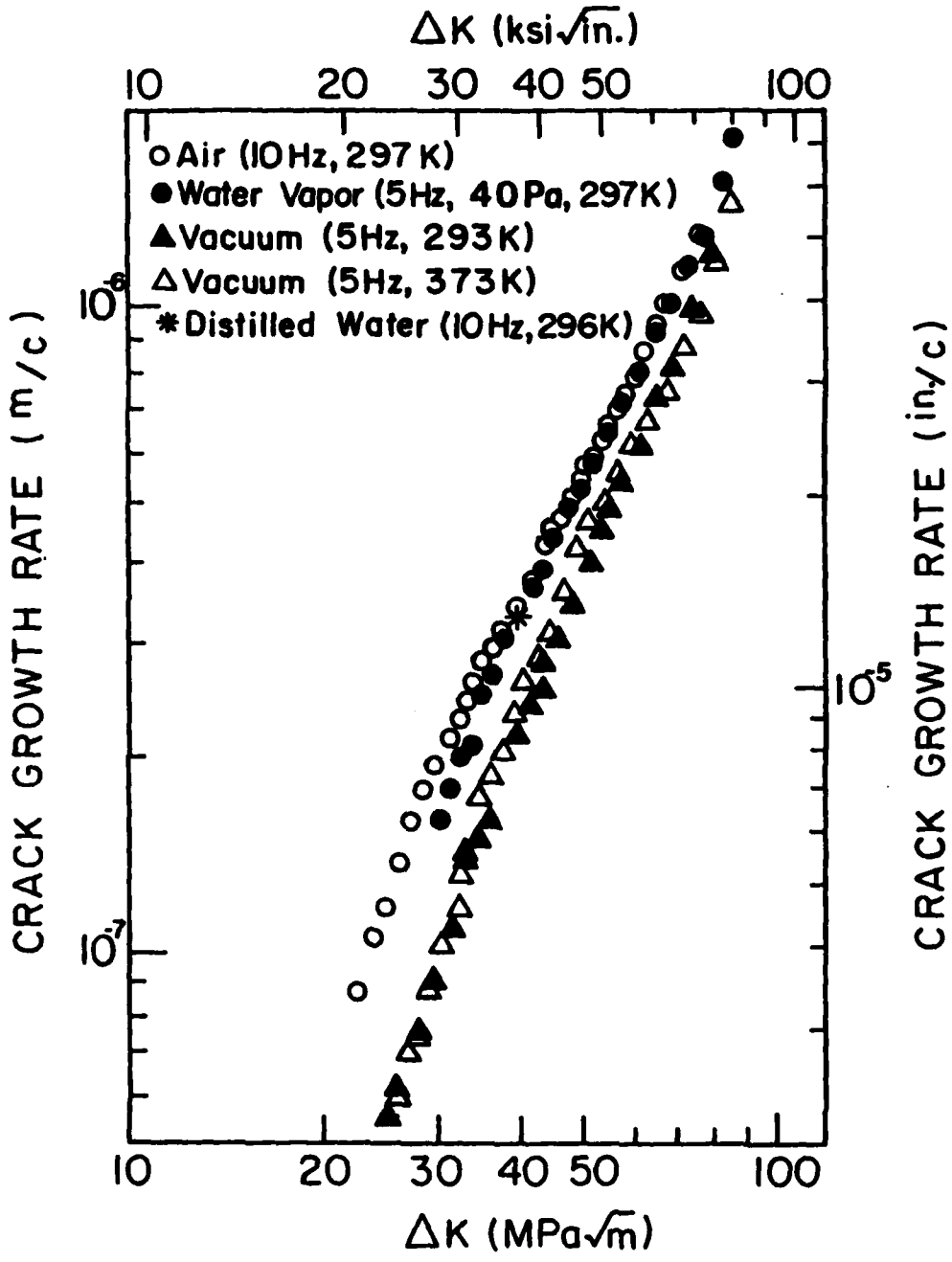

Figure 3: Crack growth data for modified HY130 steel in 40 Pa water vapor, in air, and in vacuum at 293 and 373 K. (R = 0.1 and f = 5 Hz.).

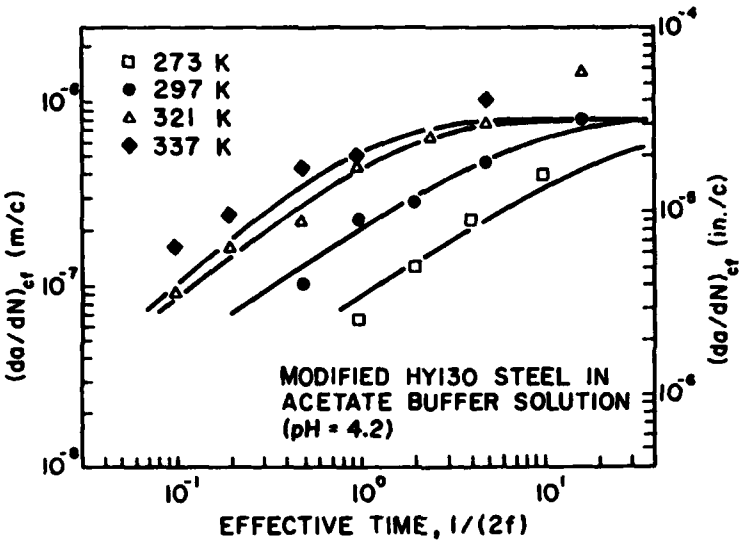

Figure 4: Correlation between crack growth rates and the fractional surface coverage by atomic hydrogen.

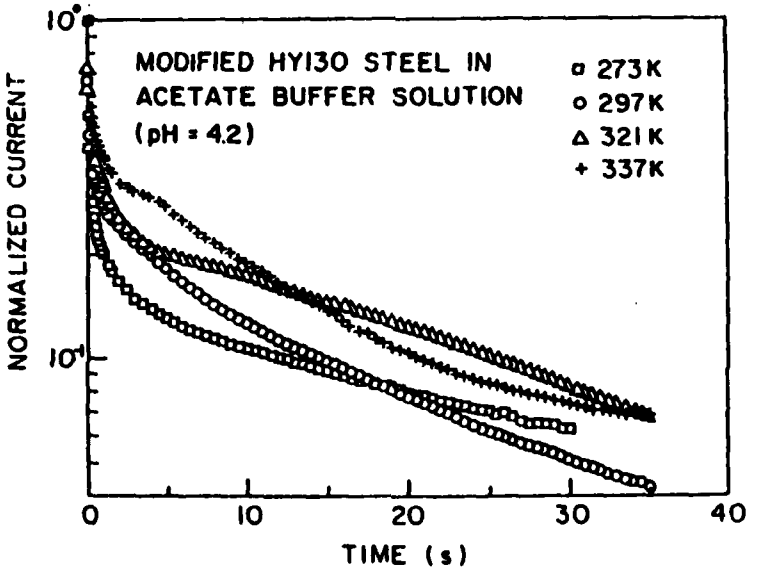

Figure 5: Semi-logarithmic representation of galvanic current transients at several temperatures.

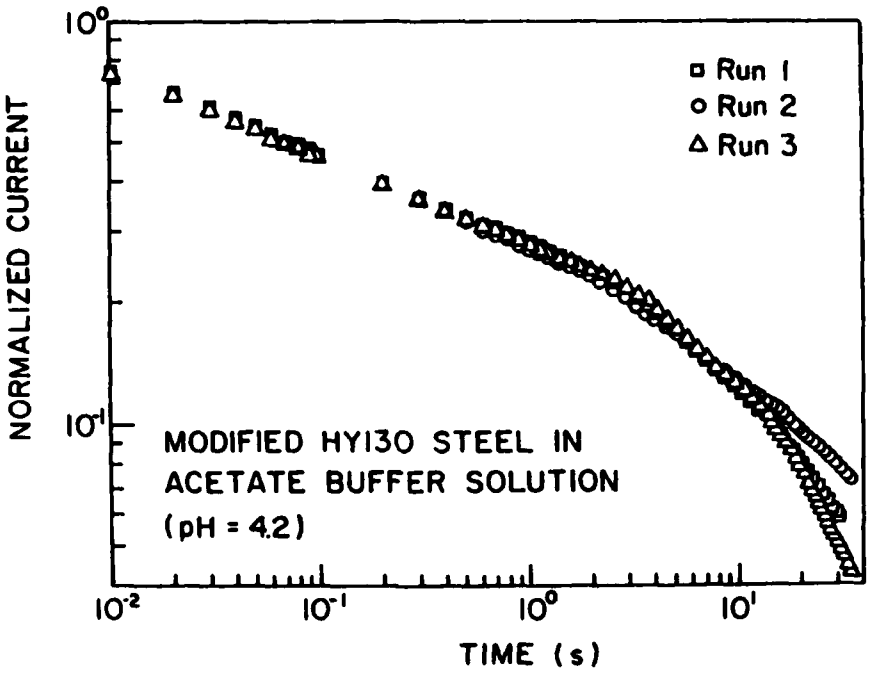

Figure 6: Galvanic current transients at 297 K.

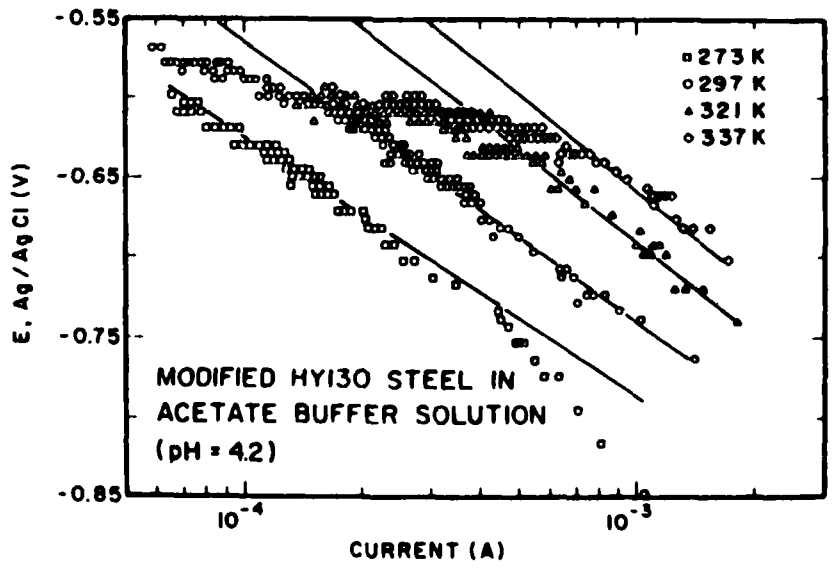

Figure 7: Current-potential relation during the transient.

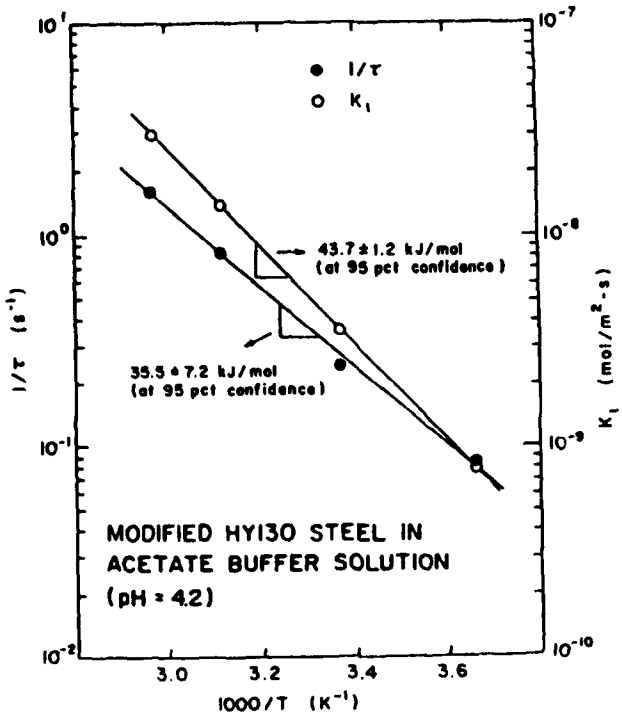

Figure 8: Temperature dependence for corrosion fatigue crack growth and for the Volmer reaction in buffered acetate solution.

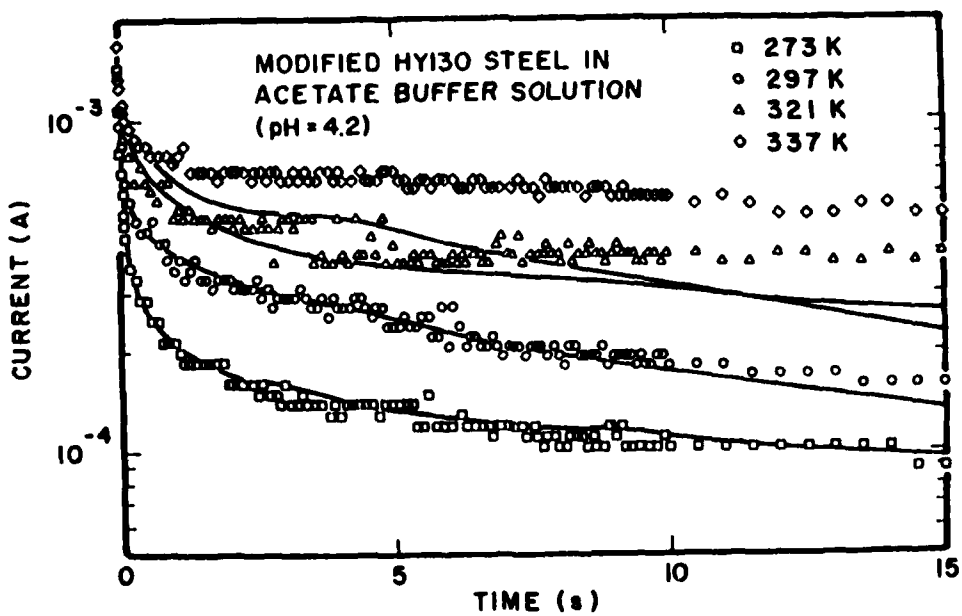

Figure 9: Comparison between measured current transients (solid curves) and the computed values from the measured potentials (open symbols).

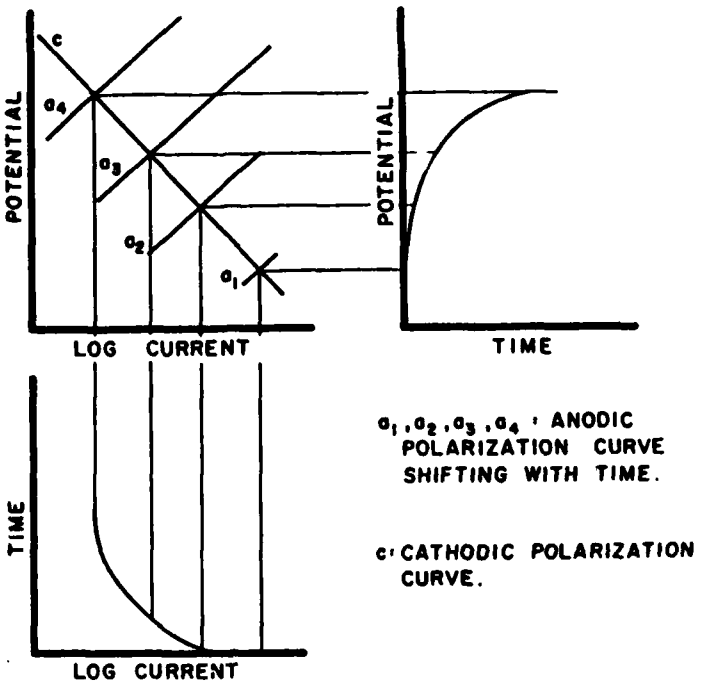

Figure 10: Schematic diagram illustrating the current-potential relation during a transient.

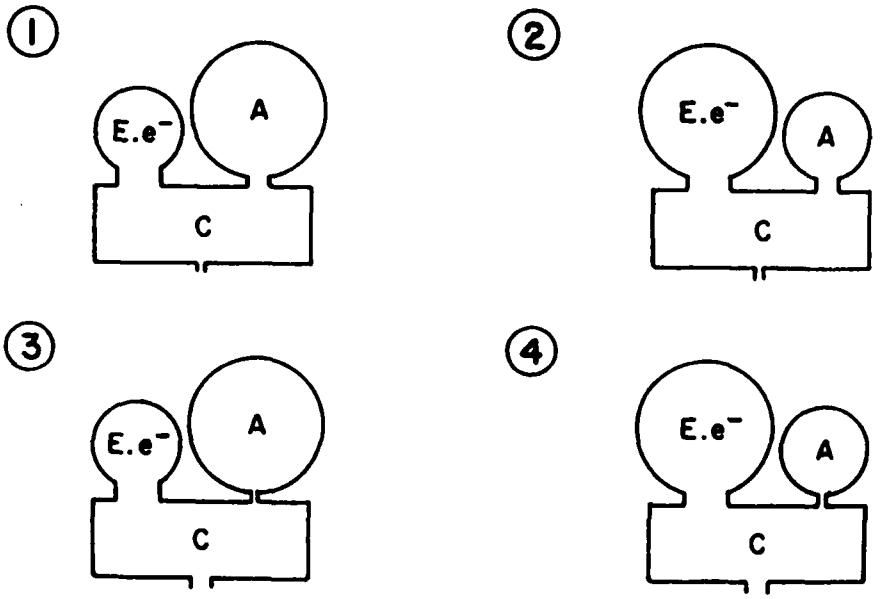

Figure 11: Four possible cases of the galvanic cell experiment with cathodic cleaning to obtain a clean surface.

E.e⁻: extraneous electrons accumulated by the cleaning process.
A : anodic reaction process.
C : cathodic reaction process.

BASIC DISTRIBUTION LIST

Technical and Summary Reports 1985

Organization	Codes
Defense Documentation Center Cameron Station Alexandria, VA 22314	12
Office of Naval Research Department of the Navy 800 N. Quincy Street Arlington, VA 22217 Attn: Code 431	3
Naval Research Laboratory Washington, DC 20375 ATTN: Codes 6000 6300 2627	1 1 1
Naval Air Development Center Code 606 Warminster, PA 18974 ATTN: Dr. J. DeLuccia	1
Commanding Officer Naval Surface Weapons Center White Oak Laboratory Silver Spring, MD 20910 ATTN: Library	1
Naval Oceans Systems Center San Diego, CA 92132 ATTN: Library	1
Naval Postgraduate School Monterey, CA 93940 ATTN: Mechanical Engineering Department	1
Naval Air Systems Command Washington, DC 20360 ATTN: Code 310A Code 5304B	1 1
Naval Sea System Command Washington, DC 20362 ATTN: Code 05R	1

Organization	Copies
Naval Air Propulsion Test Center Trenton, NJ 08628 ATTN: Library	1
Naval Construction Battallion Civil Engineering Laboratory Port Hueneme, CA 93043 ATTN: Materials Division	1
Naval Electronics Laboratory San Diego, CA 92152 ATTN: Electron Materials Sciences Division	1
Naval Missile Center Materials Consultant Code 3312-1 Point Mugu, CA 92041	1
Commander David W. Taylor Naval Ship Research and Development Center Bethesda, MD 20084	1
Naval Underwater System Center Newport, RI 02840 ATTN: Library	1
Naval Weapons Center China Lake, CA 93555 ATTN: Library	1
NASA Lewis Research Center 21000 Brookpark Road Cleveland, OH 44135 ATTN: Library	1
National Bureau of Standards Washington, DC 20234 ATTN: Metals Science and Standards Division Ceramics Glass and Solid State Science Division Fracture and Deformation Div.	1 1 1

Naval Facilities Engineering Command
Alexandria, VA 22331
ATTN: Code 03 1

Scientific Advisor
Commandant of the Marine Corps
Washington, DC 20380
ATTN: Code AX 1

Army Research Office
P. O. Box 12211
Triangle Park, NC 27709
ATTN: Metallurgy & Ceramics Program 1

Army Materials and Mechanics Research Center
Watertown, MA 02172
ATTN: Research Programs Office 1

Air Force Office of Scientific Research/NE
Building 410
Bolling Air Force Base
Washington, DC 20332
ATTN: Electronics & Materials Science Directorate 1

NASA Headquarters
Washington, DC 20546
ATTN: Code RRM 1

Defense Metals and Ceramics Information Center
Battelle Memorial Institute
505 King Avenue
Columbus, OH 43201 1

Metals and Ceramics Division
Oak Ridge National Laboratory
P.O. Box X
Oak Ridge, TN 37380 1

Los Alamos Scientific Laboratory
P.O. Box 1663
Los Alamos, NM 87544
ATTN: Report Librarian 1

Argonne National Laboratory
Metallurgy Division
P.O. Box 229
Lemont, IL 60439 1

Brookhaven National Laboratory
Technical Information Division
Upton, Long Island
New York 11973
ATTN: Research Library 1

Library
Building 50, Room 134
Lawrence Radiation Laboratory
Berkeley, CA 1

Supplemental Distribution List Jan 1985

Prof. I.M. Bernstein
Dept. of Metallurgy and Materials Science
Carnegie-Mellon University
Pittsburgh, PA 15213

Prof. H.K. Birnbaum
Dept. of Metallurgy & Mining Eng.
University of Illinois
Urbana, Ill 61801

Dr. D.H. Boone
Department of Mechanical Eng.
Naval Postgraduate School
Monterey, CA 93943

Dr. C.R. Crowe
Code 6372
Naval Research Laboratory
Washington, D.C. 20375

Prof. D.J. Duquette
Dept. of Metallurgical Eng.
Rensselaer Polytechnic Inst.
Troy, NY 12181

Prof. J.F. Hirth
Dept. of Metallurgical Eng.
The Ohio State University
Columbus, OH 43210

Dr. R.G. Kasper
Code 4493
Naval Underwater Systems Center
New London, CT 06320

Prof. H. Leidheiser, Jr.
Center for Coatings and Surface Research
Sinclair Laboratory, Bld. No. 7
Lehigh University
Bethlehem, PA 18015

Dr. F. Mansfeld
Rockwell International - Science Center
1049 Camino Dos Rios
P.O. Box 1085
Thousand Oaks, CA 91360

Profs. G.H. Meier and F.S.Pettit
Dept. of Metallurgical and
Materials Eng.
University of Pittsburgh
Pittsburgh, PA 15261

Dr. J.R. Pickens
Martin Marietta Laboratories
1450 South Rolling Rd.
Baltimore, MD 21227-3898

Prof. H.W. Pickering
Dept. of Materials Science and
Eng.
The Pennsylvania State
University
University Park, PA 16802

Prof. R. Summit
Dept. of Metallurgy Mechanics
and Materials Science
Michigan State University
East Lansing, MI 48824

Prof. R.P. Wei
Dept. of Mechanical Engineering
and Mechanics
Lehigh University
Bethlehem, PA 18015

Prof. A.J. Ardell
Dept. of Materials Science and
Eng.
School of Engineering & Applied
Sciences
University of California at
Los Angeles
Los Angeles, CA 90024

Prof. B.E. Wilde
Fontana Corrosion Center
Dept. of Metallurgical Eng.
The Ohio State University
116 West 19th Ave.
Columbus, OH 43210

Dr. C.R. Clayton
Department of Materials Science
& Engineering
State University of New York
Stony Brook
Long Island, New York 11794

END

10-86

DTIC